STUDY OF THE CORROSION RESISTANCE OF 316L STAINLESS STEEL MADE BY DIRECTED ENERGY DEPOSITION FOR APPLICATIONS AT AN ELEVATED TEMPERATURE

Alberto Alejandro Canales Cantu

Thesis Prepared for the Degree of

MASTER OF SCIENCE

UNIVERSITY OF NORTH TEXAS

December 2021

APPROVED:

Hector R. Siller, Major Professor
Seifollah Nasrazadani, Co-Major Professor
Huseyin Bostanci, Committee Member
Reza Mirshams, Committee Member
Kuruvilla John, Chair of the Department of Mechanical Engineering
Hanchen Huang, Dean of the College of Engineering
Victor Prybutok, Dean of the Toulouse Graduate School

Canales Cantu, Alberto Alejandro. *Study of the Corrosion Resistance of 316L Stainless Steel Made by Directed Energy Deposition for Applications at an Elevated Temperature*. Master of Science (Engineering Technology), December 2021, 45 pp., 13 tables, 32 figures, 1 appendix, 27 numbered references.

The corrosion resistance under elevated temperature of additively manufactured 316L stainless steel made by directed energy deposition was studied. Test samples were prepared in a hybrid additive manufacturing machine using standard deposition parameters recommended by the manufacturer. Control samples were cut from wrought material to compare the results. The test was performed under a corrosive atmosphere with a solution of water with 3.5 % in weight of salt (NaCl). The total duration of the test was 635 hours, divided in five stages of 12, 24, 48, 226, and 325 hours to analyze the samples between each stage. The samples were analyzed quantitatively measuring weight loss and surface topography, and qualitatively by macroscopic inspection with digital photography, and microscopic inspection with optical and scanning electron microscopy. The results show a higher corrosion rate for the additively manufactured samples compared to the control samples. An evident increase in the size of pits initially present on the samples was observed and quantified on the additively manufactured. Although the additively manufactured samples were more aggressively attacked by corrosion, they still presented a shiny surface finish at the end of the test, reinforcing the idea of the formation of a passive oxide layer and suggesting that the corrosion was focalized in the surface defects by pitting and crevice corrosion mechanisms.

ACKNOWLEDGMENTS

To my major professor, Dr. Hector R. Siller, and to the University of North Texas, for granting me the opportunity to work here and get this degree. To Dr. Leticia Anaya, for trusting in my capabilities and supporting my appointment as teaching assistant. To Dr. Seifollah Nasrazadani, for his help and advice as chair of the department and director of the graduate program in Engineering Technology, as my teacher in the topic of corrosion, and as my co-advisor. To my co-advisor and teacher, Dr. Huseyin Bostanci, for his guidance and provision of materials and facilities to perform this research. To Dr. Reza Mirshams, for his feedback to improve this work. To the Center for Agile & Adaptive and Additive Manufacturing (CAAAM) funded through State of Texas Appropriation #190405-105-805008-220 at the University of North Texas, for their infrastructure and support. To Dr. Narendra Dahotre, for providing access to their cutting-edge equipment which was crucial for the execution of this research work. To Emerson Automation Solutions that provided material for the experimentation. To Bobby Grimes and his team, for all the technical support and troubleshooting. To my friends and colleagues, Cesar Chavez, Jashim Uddin, Zane Hughes, and Christopher Haney, for their substantial contributions in the operation and training on the use of the specialized equipment critical to this investigation.

To my mom, my sister, my brother-in-law, my niece Helena, my nephew Antonio, my father, and our loved nanny Juany, for their support in this pursuit. To my friends, old and new, for making the road smoother and happier. A final special acknowledgement to my counselor Nancy Rodriguez, for her guidance in the transition to follow this aspiration.

I dedicate this work to my grandma Elena, who encourages me even during her physical absence. With all the love, thank you.

TABLE OF CONTENTS

Page

LIST OF TABLES

Page

LIST OF ILUSTRATIONS

Page

CHAPTER 1

INTRODUCTION

Additive manufacturing (AM) refers to the processes for making parts by adding material in superposed layers until the desired shape is gotten. Although its origin of is not recent, it still presents several areas of opportunity for optimization in process control and manufactured products performance, so there is a huge opportunity for research to improve the capabilities of the different AM processes and increase their industrial and domestic applications. The trends of investigation comprise new AM materials development, AM parts mechanical properties, process optimization and reliability, AM products quality inspection, and potential uses of AM. One potential use that will generate high impact in the industry is the manufacturing of components for flow systems, like valves and piping elements.

Any industrial plant in the world possess complex piping systems that operate continuously, and their failure causes huge losses due to forced operation stops for repair. This problem is exacerbated in the oil and gas, and nuclear power industries, which work under high demanding thermal and flow conditions. With the use of directed energy deposition (DED), it could be possible to rapidly manufacture replacements for the damaged sections or even perform the repair on-site over the damaged pipeline. Nevertheless, as any novel technology, there are still unknowns regarding the capabilities and process parameters control to achieve a material with competitive performance or superior to current materials in market produced by conventional manufacturing processes.

Directed energy deposition consists in feeding a controlled amount of metallic wire, filament, or powder, that is immediately heated and melted by a laser ray or electron beam

(focused thermal energy) shot over a substrate in a continuous process [1]. Usually, both the metal feeder and the focused thermal energy source are built into a single nozzle which also feeds an inert gas to create a protective atmosphere to inhibit corrosion of the molten metal. As the nozzle advances and the metal solidifies, a track or layer of material is formed. The process is iterated over the previously deposited track until the desired material geometry is obtained. The main parameters controlled in this process are laser power, laser scanning speed, track overlap, and powder feed rate (Fig. 1).

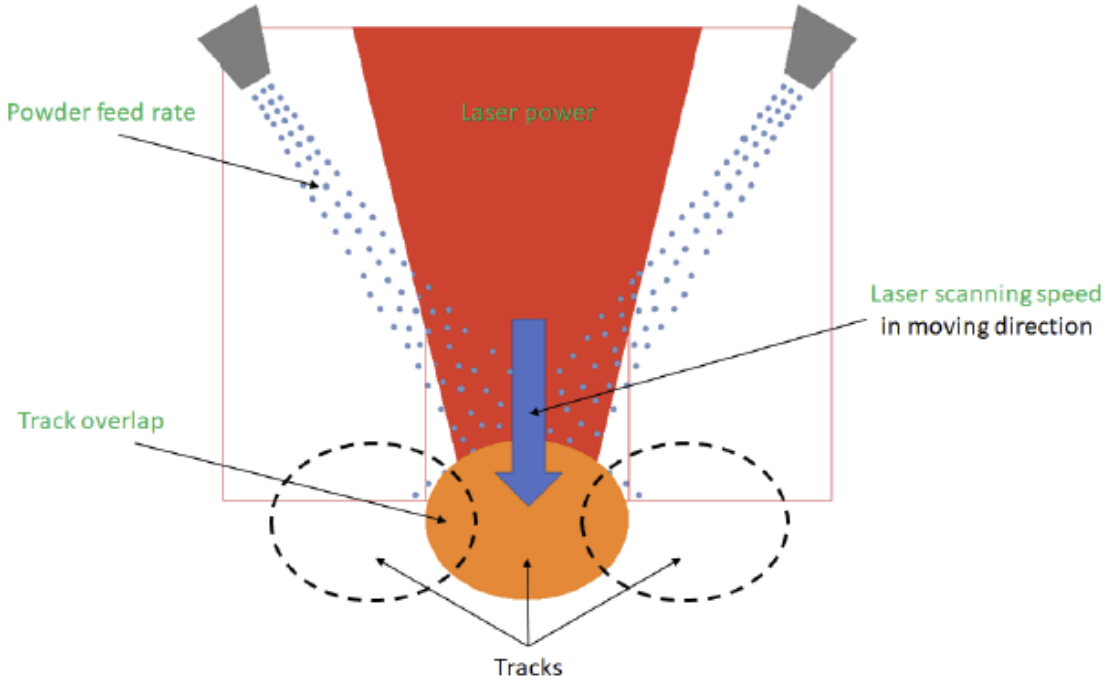

Figure 1: Schematic of the directed energy deposition (DED) process.

The proposed research is focused on evaluating the corrosion resistance under elevated temperature and humidity conditions of 316L stainless steel made by directed energy deposition additive manufacturing, in contrast to the material made by conventional methods, as an initial step to assess the feasibility of using this technology for the production of components for flow systems and for on-site repairs of industrial pipelines, machinery, and structures.

CHAPTER 2

LITERATURE REVIEW

A literature review has been performed, covering applications for additive manufacturing (AM) and hybrid AM, current technologies and equipment for AM, metrology applied to evaluate AM topographies, industrial cases of failure of systems working under high temperature and humidity, failure modes presented under high temperature and humidity, and evaluation of corrosion resistance and mechanical properties of additively manufactured 316L stainless steel. These topics are of interest for the present research because a hybrid additive manufacturing machine was used for the experimental work, and surface evaluation technology was used for the analysis of test samples. The origin of the papers spans from the USA, the UK, France, Sweden, Italy, and Iran, which indicates that the topic is a current trend of research worldwide. No matter that AM is being applied in an increasingly number of companies of different background, it is still a novel technology. A lot of research is needed and currently being conducted to improve the understanding of the dynamics of the deposition process, process control, and parts quality evaluation.

2.1 Additive Manufacturing and Areal Topography Inspection

As general reference of the technology used for the current research, the following sources were consulted.

Sealy et al. [2] point out in their review of hybrid processes in additive manufacturing, hybrid manufacturing can be studied from the basis of the process, the machine, and the product. A hybrid process comprises the combination of two different technologies that work synergistically and cannot be decoupled to achieve the desired output, i.e., the fabrication of a

part, and have effect over the part quality, functionality, or process performance. A hybrid machine is one in which two or more different processes or energy sources work independently, not necessarily simultaneously, to produce the output. Last, a product can have hybrid material, i.e., made of two or more different materials; hybrid structure, i.e., different microstructure along its body, or hybrid function, have two or more functionalities embedded in one single part, produced in a single build. With those definitions, hybrid AM can be defined as hybrid AM processes, hybrid AM machines, and hybrid AM products. The following hybrid AM (HAM) processes are identified: HAM by machining, HAM by ablation or erosion, HAM by re-melting, HAM by laser assisted plasma deposition, HAM by peening, HAM by rolling and burnishing, and HAM by friction stir processing. All of these HAM processes, involve the mentioned process working synergistically and coupled with AM.

A study of the geometries possible to achieve on heat exchangers is presented on the white paper by Stratasys [3], which show researches about thin film cooling, and improved pin fin geometries. Thin film cooling works by the creation of a thin layer of a cold fluid in the interface between a hot and a cold process. By the generation of holes on the pipe walls of the cold chamber, a minimal flow is allowed out to the outer surface which is in contact with the hot process. With AM, the holes can be created during the formation of the part, eliminating the necessity for postprocessing. Another possibility for enhancing the performance of heat exchangers is the use of pin fins with variable geometry. Using AM, the parts can be created with the pin fins in a single build.

Townsend et al. [4] presented a list of techniques used for AM surfaces inspection i.e., areal topography measurement. Thompson et al. and Cabanettes et al. [5], [6], made a more in-

depth work, assessing different measuring techniques. This is an important aspect to consider for controlling AM surface roughness and therefore part quality. The irregular surfaces obtained with this family of processes present significant challenges for profile and texture evaluation using the industry standard tools e.g., contact profilometers. The most relevant technologies evaluated are coordinate measuring machine (CMM), confocal microscopy (CM), scanning electron microscopy (SEM), focus variation microscopy (FVM), coherence scanning interferometry (CSI), and X-ray computed tomography (XCT). The results suggest that FVM, CSI, and XCT deliver the most accurate areal topography measurements, although FVM and XCT present some problems detecting deep valleys and high peaks.

2.2 Directed Energy Deposition Process Parameters Control

Keshavarzkermani et al. [7] conducted a research on the influence of the variation in laser energy density (LED), laser power, and scanning speed, on the melt pool dimensions and its corresponding microstructure. They found that the laser power has a greater impact than the scanning speed on the obtained melt pool. If the scanning speed is kept constant, an increase in the laser power generates a deeper and wider melt pool. On the other hand, if the power is kept constant, a reduction in the scanning speed will increase both dimensions of the melt pool but in a smaller fraction. Also, for a fixed LED, higher values of power produce a greater impact than varying scanning speed on increasing the melt pool size. Another relevant aspect presented on the research is the microstructure of the melt pool. It was found that higher laser power promotes new nucleation sites as it influences the generation of a bigger partially melted zone on the surrounding of the laser beam, where grains detach from the boundary of solid metal and move into the melt pool creating more sites for growth and therefore a finer microstructure.

Saboori et al. [8] studied the effect of powder recycling on the microstructure and consequently on the tensile strength of 316L stainless steel produced by directed energy deposition. This is relevant to consider the healthy span and establish best practices of use of powder for depositions.

In another paper, Saboori et al. [9] report that the presence of oxides which are detrimental to the performance of 316L stainless steel, is lower in material produced by DED compared to material produced by conventional methods. Moreover, they point the importance of controlling the protective gas feed during the deposition process, to provide an adequate protective atmosphere to reduce the formation of these oxide particles and achieve the full potential of the material, both in terms of mechanical properties and corrosion resistance.

2.3 Comparison to Similar Technologies

Other processes have the capabilities for producing structures in a similar manner than directed energy deposition (DED). Wire arc additive manufacturing (WAAM) is one process that has presented considerable development and is one of the main competitors of DED. WAAM works under the principles of gas metal arc welding, where an electric arc melts a wire that provides the metal for the deposition under an inert gas atmosphere. Subsequent tracks are deposited one over another to produce the desired geometry; this is controlled by a robotic arm. A schematic of WAAM is shown in Figure 2.

A comparison between DED and WAAM is presented in Table 1.

Table 1: Comparison between Directed Energy Deposition and Wire Arc Additive Manufacturing technologies. Sources: [8]–[12].

Technology	Advantages	Disadvantages
WAAM	Large scale parts.	Not suitable for applications requiring precise deposition in verry small areas. Size of tracks is constrained by the gage of wire.
	Cheaper materials. Uses standard welding supplies.	Lower material variety compared to DED. Constrained by welding supplies available in market.
	Cheaper equipment. Uses conventional welding equipment.	Lesser material versatility compared to DED. Materials cannot be mixed in a single track. Odd layers of different materials can be deposited, but a stop for tool setup or several deposition heads are required.
	Easier setup. No special personal protective equipment required to perform material setup or restock.	
	Denser deposited material without the necessity of postprocessing (heat treatment).	
	Competitive level of mechanical properties compared to conventional manufacturing processes (Ys 418 MPa according to [11]).	
DED	Small to medium scale parts.	More expensive supplies (powder).
	Competitive level of mechanical properties compared to conventional manufacturing processes (Ys 450-550 MPa according to [8], [9]).	More expensive equipment compared to WAAM.
	Very high cooling rates which produce finer microstructures and better mechanical properties.	Special personal protective equipment and special room required for powder handling and storage.
	Higher variety of materials in market compared to WAAM.	Deposited material can present high porosity and postprocessing (heat treatment) is needed to reduce porosity and increase mechanical properties.
	Hybrid materials. Different powders can be mixed for a single deposition or layers of different materials can be subsequently deposited without any setup.	Lower ductility than conventional manufacturing processes.
	Material can be deposited in very small areas. Good for filling small gaps, cracks, or pores.	Anisotropic tensile properties.

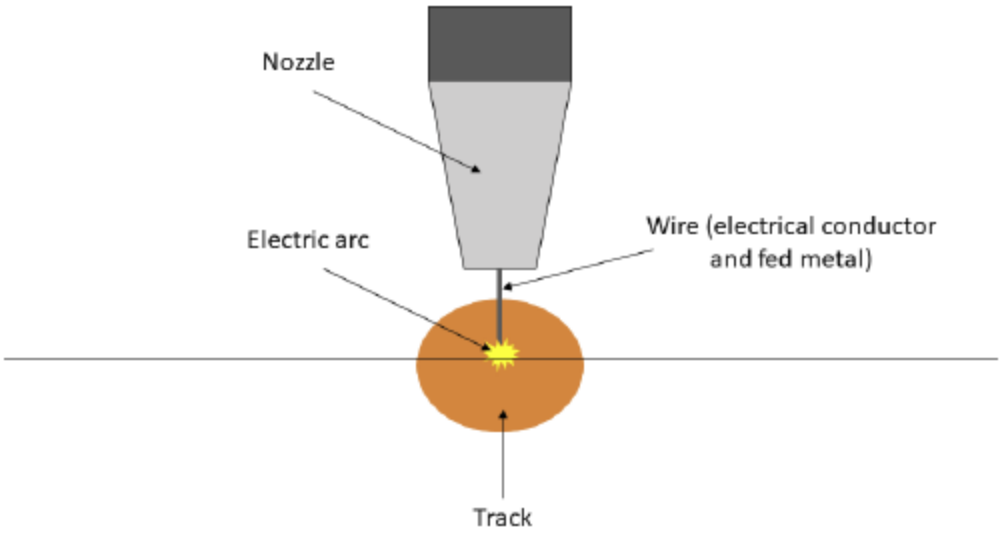

Figure 2: Schematic of wire arc additive manufacturing process (WAAM).

2.4 Failure Modes of Industrial Elements Under Elevated Temperature Conditions

Lou et al. [13], [14] investigated the tendency to stress corrosion cracking in high temperature water (288°C) of 316L stainless steel AM samples produced by laser powder bed fusion method and postprocessed under different heat treatments and cold work. They concluded that high temperature annealing recrystallization improved the stress corrosion cracking behavior of the samples, providing good material properties for use in nuclear applications. Although the AM technology used on their research is different than DED, it provides a good reference for the current work.

Bagheri, Nasrazadani, and Bostanci [15], conducted a research about the impact of internal grooves on the accelerated wear of pipes due to the modification of the flow pattern. This is important to consider for evaluating the use of DED technology for repair of this kind of parts.

Kain [16] reported different types of FAC in case studies of nuclear power plants piping systems, following the well-known classification of single phase and dual phase flow, and

presented a special case of the later one known as liquid droplet impingement (LDI) or shotgun pattern corrosion. LDI is caused by small droplets of liquid that are dragged by the vapor phase and projected to the pipe walls, damaging the protective oxide layer. It is pointed that LDI is prone to occur in elbows (bends of piping) due to the change in the direction of the flow. Another important point presented in the article is that 316L stainless steel is highly resistant to FAC and previous laboratory tests reported negligible rates of this corrosion mechanism for the material, therefore suggesting it as a highly recommended option for substituting damaged sections of pipelines. It was also recommended to use pipes and fittings of higher schedule than required on critical parts of the system prone to FAC. The maximum FAC rate was found to be in water with a pH of 9.5 and a temperature of 150°C.

2.5 Corrosion Evaluation

To define the experimental methodology and the presentation of results of the current research, a review was done of several previous studies about corrosion evaluation of 316L stainless steel and of metals produced by additive manufacturing methods. Of these investigations, one of the most relevant which was used as a reference for the present research is the performed by Dhaiveegan et al. [17] about the corrosion resistance of 316L and 304 stainless steel in an urban environment. They made an experiment exposing the materials to the open atmosphere in a city with the conditions described and analyzed the materials weight loss and change in mechanical properties. Other relevant work which helped as a reference for analyzing the features observed in the visual evaluation of the samples, is the research performed by Ganesh et al. [18] about pitting corrosion on 316L stainless steel made by laser rapid manufacturing, which is a technique that works on similar principles to DED. They compared the

occurrence of this kind of corrosion mechanism in samples produced by AM and by conventional methods, and comment on the causes that trigger it.

Ko et al. [19] present a comprehensive review of published investigations on corrosion of AM stainless steel (various grades), providing a useful reference for the development of new researches. Several additional publications reviewed for the current work provide insight to the physicochemical and optical techniques used to characterize the corrosion effects and products, and highlight the good performance of AM 316L stainless steel under different corrosive conditions; these sources are summarized in Table 2.

2.6 Research Questions

How does 316L stainless steel made by DED perform compared to conventional manufacturing methods, in terms of corrosion resistance and produced parts integrity in as manufactured state and after use under severe corrosive conditions?

Hypothesis: It is hypothesized that parts made of 316L stainless steel by DED AM, can perform consistently in terms of corrosion resistance and material integrity, and be an alternative to conventionally made components.

Table 2: Previous investigations about corrosion resistance of 316L stainless steel and other metals produced by additive manufacturing and conventional methods.

Manufacturing process	Material	Controlled parameters	Relevant feature	Corrosion characterization method	Reference
Wrought	316 SS, Inconel 325	Temperature, time	Nickel content	WL, SEM, EDX, XRD, PDP, EIS	[20]
AM (not specified)	316L SS	pH	Passive oxide film	SEM, XPS, EDX, XRD, EIS	[21]
SLM	316L SS	Corrosive agent concentration	Oil and gas industry environment, Pitting resistance, passive oxide film	XRD, SEM, EDX, PDP, PSP, EIS	[22]
SLM, DED	316L SS	Manufacturing process (SLM, DED)	Passive film formation, grain size	PDP, OM, SEM, EDS, AFM	[23]
LPBF	316L SS	Heat treatment, crack orientation, cold work	Corrosion fatigue crack growth, high temperature nuclear applications, microstructure control	SCCGR, EBSD, SEM, TT	[13]
LPBF	316L SS	Heat treatment, cold work, rolling direction, porosity, build direction, loading direction, stress intensity,	Stress corrosion cracking, porosity, microstructure control, AM post-processing heat treatments, nuclear applications, high temperature water (288° C)	SCCGR, SEM, BSE, EBSD	[14]
SLM	316L SS	Powder particles size	Corrosion tendency vs corrosion rate, corrosion progression, passive oxide film, pitting corrosion, crevice corrosion	WL, PDP, OM, SEM, EDX, XRD	[24]
SLM	316L-1 wt.% NiB SS	Scanning speed, pulse energy, power, pulse length, hatch distance, layer thickness	1 wt. % NiB addition, microhardness increase	DF, OM, SEM, OP, MH, WL	[25]

*Explanation of acronyms of materials: AM additive manufacturing, DED directed energy deposition, LPBF laser powder bed fusion, SLM selective laser melting. *Explanation of acronyms of tests: WL weight loss, SEM scanning electron microscopy, OM optical microscopy, EDX energy dispersive X-ray spectroscopy, XRD X-ray diffraction, EIS electrochemical impedance spectroscopy, XPS X-ray photoelectron spectroscopy, PDP potentiodynamic polarization, PSP potentiostatic polarization, AFM atomic force microscopy, SCCGR stress corrosion cracking growth rate, EBSD electron back scattered diffraction, TT tensile test, BSE back-scattered electron, DF digital photography, OP optical profilometry, MH microhardness.

CHAPTER 3

METHODOLOGY

For the execution of this research work, which included the utilization of several equipment and materials for the test setup, preparation of samples, testing, and analysis, many activities were performed which can be described in stages. Those stages of the research are described in Figure 3.

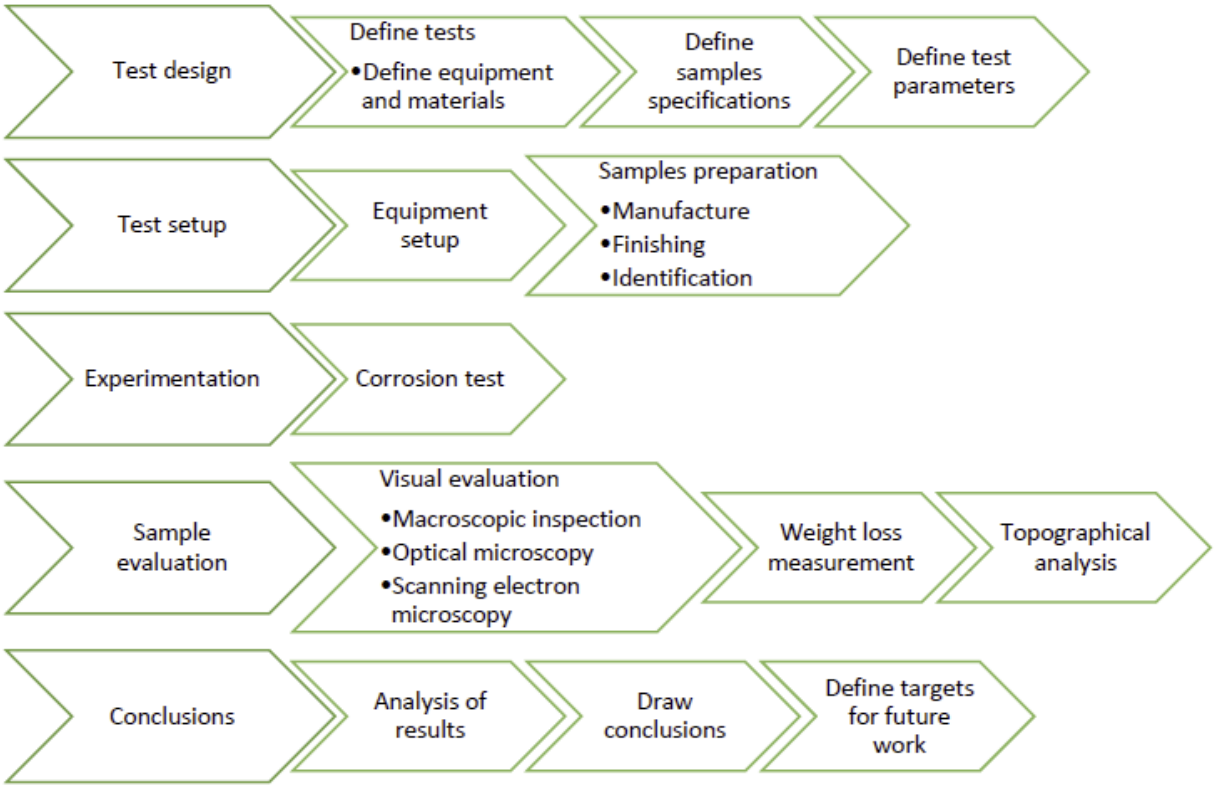

Figure 3: Diagram of stages of the present research.

For the experiment, rectangular samples of 316L stainless steel were prepared and tested under a corrosive atmosphere of a solution of water and 3.5% NaCl at high temperature, using an autoclave. The samples were quantitatively and qualitatively analyzed after the tests, evaluating the material loss, the corrosion products generated, and the changes to their morphology.

3.1 Test Description

To test the resistance to corrosion of additively manufactured 316L stainless steel, four rectangular sections of this material and same number of control samples from wrought material were prepared and subjected to a corrosive atmosphere of salty water steam. The oxide formation was evaluated quantitatively and qualitatively through weight and volume variation measurement, visual inspection, optical microscopy, and scanning electron microscopy.

3.2 Sample Preparation

Rectangular sections of 316L stainless steel were additively manufactured by directed energy deposition using 316L austenitic stainless-steel powder manufactured by LPW (chemical composition on Table 3). The deposition parameters are shown on Table 4. The machine used for the deposition is a Hass Mini Mill equipped with a Hybrid Ambit Multi directed energy deposition system with an Ytterbium laser system from IPG (Fig. 4). A flat plate of 302 stainless steel with a standard thickness of 5/16 inches (measured 7.874 mm) was used as substrate. The section with the deposited tracks was cut using wire electro-discharge machining, and following, the samples were detached using the same process making a cut parallel to the surface (Fig. 5). The cuts were done in a Mitsubishi MV1200S wire EDM machine (Fig. 6). The detached samples were sanded using 120 grid, 240 grid, and 1200 grid SiC abrasive paper at 100 rpm, and polished with 5 micrometers and 0.05 micrometers alumina at 250 to 350 rpm (Fig. 7). The samples dimensions after cut, sanding, and polishing are reported on Table 5.

Table 3: Chemical composition of 316L austenitic stainless-steel powder manufactured by LPW, used for producing the corrosion test samples.

C %	Cr %	Cu %	Mn %	Mo %	N %	Ni %	O %	P %	S %	Si %
0.03	17.5 – 18.0	0.5	2.0	2.25 – 2.5	0.10	12.5 – 13.0	0.1	0.025	0.01	0.75

Table 4: DED process parameters for manufacture of test samples.

Power (W)	Scanning speed (mm/min)	Overlap (1-stepover)	Powder feed rate (g/min)
300	350	0.65	3

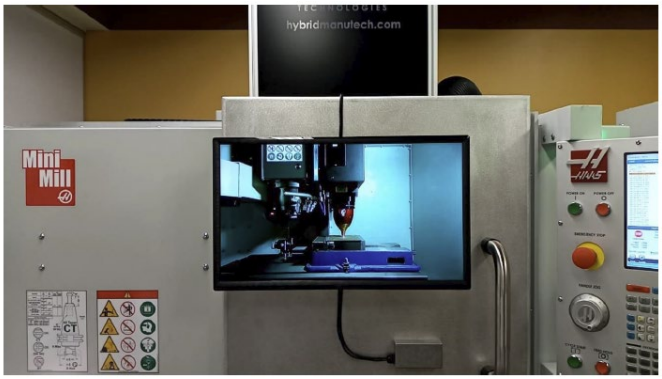

Figure 4: Hass Mini Mill equipped with a Hybrid Ambit Multi directed energy deposition system with Ytterbium laser from IPG, used for the manufacture of the test samples.

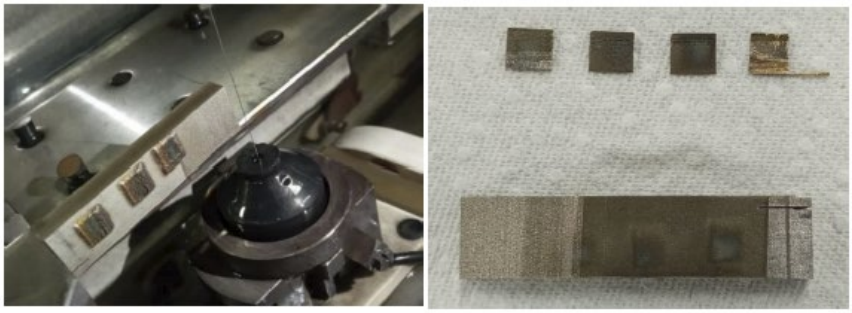

Figure 5: AM samples for corrosion test being detached from substrate using wire electro-discharge machining (left) and after being detached (right).

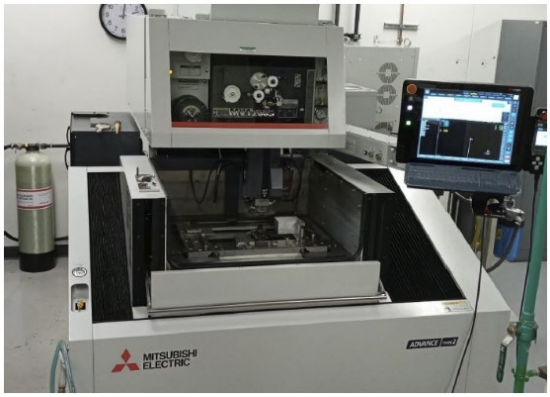

Figure 6: Mitsubishi MV1200S wire electro-discharge machine used for the preparation of samples for the corrosion test.

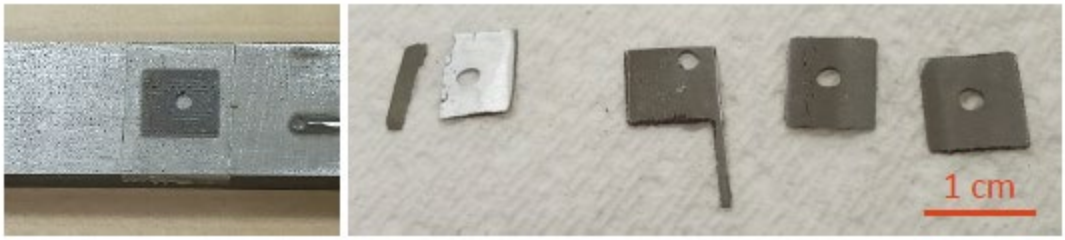

Figure 7: AM sample for corrosion test mounted for polishing after cut on wire EDM (left). Set of AM samples during polishing process; one sample fractured during the process (right).

Table 5: AM test samples dimensions measured using a vernier caliper and their calculated total surface area.

Sample	Length (mm)	Width (mm)	Thickness (mm)	Hole Diameter (mm)	Total Surface Area Calculated (mm^2)
~~1*~~	~~9.14~~	~~Unable to measure~~	~~0.28~~	~~1.66~~	~~------~~
2	7.66 (+arm 8.58)	7.92 (+arm 1.00)	0.44	1.68	158.084 (132.934 + arm 25.1504)
3	8.98	7.60	0.38	1.66	146.750
4	9.04	8.00	0.36	1.70	154.292

* Sample 1 broke during sanding process. Reported dimensions are remaining section. Sample discarded from analysis.

The control samples were obtained from a hot rolled and annealed plate of 316L stainless steel (chemical composition on Table 6) with a standard thickness of 3/8 inches (measured 9.398 mm) with certificate of stress corrosion cracking testing. The samples were cut by wire electro—discharge machining, and sanded and polished following the same procedure, materials, and parameters used for the test samples (Figs. 8 and 9). The dimensions of the control samples after cut, sanding, and polishing are reported on Table 7.

Table 6: Chemical composition of 316L stainless steel plate used to obtain the control samples for the corrosion test.

C %	Cr %	Cu %	Mn %	Mo %	N %	Ni %	Co %	P%	S %	Si %
0.02	16.74	0.49	1.36	2.04	0.07	10.04	0.116	0.03	0.024	0.44

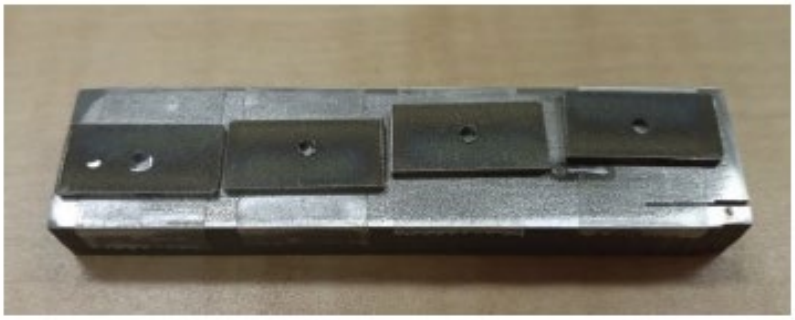

Figure 8: Control samples for corrosion test mounted for sanding and polishing.

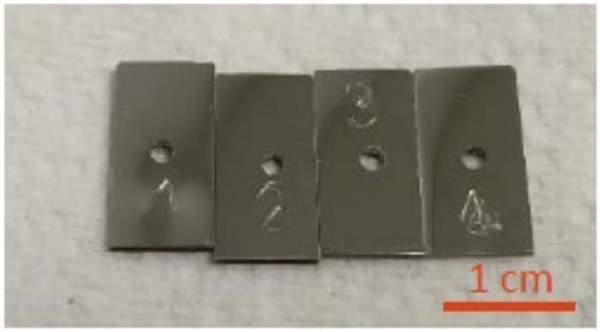

Figure 9: Control samples for corrosion test after being polished and marked for identification.

Table 7: Control samples dimensions measured using a vernier caliper and their calculated total surface area.

Sample	Length (mm)	Width (mm)	Thickness (mm)	Hole Diameter (mm)	Total Surface Area Calculated (mm^2)
1	19.70	9.40	1.00	1.70	429.361
2	19.70	9.52	1.00	1.70	434.329
3	19.70	9.40	1.00	1.72	429.316
4	19.70	9.40	1.00	1.70	429.361

The general formula used to calculate the total surface areas of both kind of samples, with exception of AM sample 2, is shown on Equation 1. In the formula, w is the width, L is the length, ϕ is the diameter of the hole, and t is the thickness. For AM sample 2 and additional part has to be added to include the arm of the sample.

$$A = \left[w.L - \pi\left(\frac{\phi}{2}\right)^2\right].2 + (2.w + 2.L).t + \pi.\phi.t \qquad \text{Eq. 1}$$

3.3 Test and Analysis

The samples were tested in an All American 25X autoclave (Fig. 10) using a solution of water with 3.5% in weight of salt (NaCl) within a temperature range of 115° C to 120° C (constant) and the corresponding pressure range between 0.7 and 1.0 Kg/cm^2 (constant) for 635 hours divided in five stages of 12, 24, 48, 226, and 325 hours. In the autoclave, the samples were suspended using nylon wires attached to aluminum bars supported on an aluminum container to avoid any potential effect of galvanic corrosion (Fig. 11). The water-salt solution was prepared weighing 4825 ml (1 ml = 1 g) of water and 175 g of salt before each test stage, using an OHAUS Valor 1000 Series scale (Fig. 12). Liquid level was verified and replenished during planned stops. The solution was stirred before pouring it into the autoclave. Before and after each corrosion test stage, the samples were weighed using an Adam PW184 analytical balance to determine their change in weight; five measurements per sample were made and recorded on each stage. Before weighing, the samples were ultrasonically cleaned with water for 10 minutes using a Branson 1510 ultrasonic cleaner and left to dry for at least 24 hours in a sealed container with moisture absorbent material. The samples were manually measured using a vernier caliper before the corrosion test and their surface area was calculated. The topographical changes on the samples were evaluated using an Alicona InfiniteFocusSL optical 3D measurement system based on focus-variation microscopy (Fig. 13). The oxide formation on the samples was documented macroscopically through standard digital photography, and microscopically through optical microscopy and scanning electron microscopy. The microscopes used are a Nikon Eclipse MA 100 optical microscope and a FEI Quanta 200 scanning electron microscope.

Figure 10: Autoclave used for the experiment. Model: All American 25X.

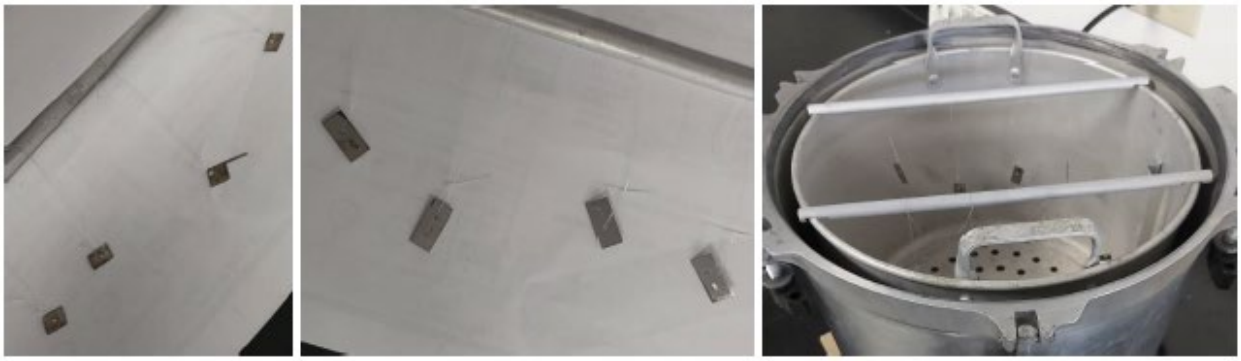

Figure 11: AM test samples (left) and control samples (center) attached to aluminum bars with nylon wires to be suspended inside the autoclave (right).

Figure 12: Measuring water (left) and salt (center) to prepare water- 3.5 wt.% NaCl solution for corrosion test. Verification of liquid level in autoclave during planned stop (right).

Figure 13: An Alicona InfiniteFocusSL optical 3D measurement system based on focus-variation microscopy, was used to obtain topographical information of the samples.

CHAPTER 4

RESULTS

4.1 Weight Loss Analysis

The average weight of the five measurements of each sample on each stage was used to calculate the change in weight per unit of surface area per exposure time to describe the change in weight due to corrosion occurred during the experiment (Table 8 to Table 11). The intermediate times between the reported were discarded because they presented bigger dispersion of the data points and there was physical reason known that could have potentially affected the measurements, causing them to be unreliable. Also, AM sample 1 was discarded from the analysis considering that it was fractured during the sanding process leaving one of its edges considerably irregular, not allowing to get an accurate measurement of its dimensions. The complete data recorded of the weight of the samples during each stage, including the discarded, are presented in the appendix.

Table 8: Average of weight measurements at different exposure times of AM samples.

Time (h)	Weight (g)			
	AM Sample 1 (discarded)	AM Sample 2	AM Sample 3	AM Sample 4
0	~~0.08810~~	0.18060	0.15858	0.16664
84	~~0.08814~~	0.18024	0.15844	0.16658
635	~~0.08772~~	0.18008	0.15826	0.16602

By subtracting the final weight to the initial weight, the change in weight is calculated. Since it is expected to see a weight reduction, the operation is done in that order to get a positive number and plot the data in the positive vertical axis as weight loss. The obtained value is then divided by the total surface area of the sample. For this case it was decided to also report the

average of the weight losses of each set of samples, to use it as a comparison index of the corrosion.

Table 9: Estimation of the weight loss of the AM samples, obtained from the average weights.

	~~AM Sample 1~~ (discarded)	AM Sample 2	AM Sample 3	AM Sample 4
Final weight loss after 635 hours ΔW (μg)	Discarded	520.0000	320.0000	620.0000
Surface Area A_o (mm^2)	Discarded	158.0840	146.7500	154.2920
ΔW/Ao (μg/mm^2)	Discarded	3.28939	2.18058	4.01835
Average Final Weight Loss per Surface Area (μg/mm^2)	3.16277			

Table 10: Average of weight measurements at different exposure times of control samples.

Time (h)	Weight (g)			
	Control Sample 1	Control Sample 2	Control Sample 3	Control Sample 4
0	1.05284	1.13784	0.93442	1.01728
84	1.05296	1.13780	0.93438	1.01738
635	1.05254	1.13754	0.93422	1.01692

Table 11: Estimation of the weight loss of the control samples, obtained from the average weights.

	Control Sample 1	Control Sample 2	Control Sample 3	Control Sample 4
Final weight loss after 635 hours ΔW (μg)	300.0000	300.0000	200.0000	360.0000
Surface Area A_o (mm^2)	429.3610	434.3290	429.3160	429.3610
ΔW/Ao (μg/mm^2)	0.698713	0.690721	0.465857	0.838455
Average Final Weight Loss per Surface Area (μg/mm^2)	0.673437			

The ratio between the results is calculated as follows:

$$Corrosion\ ratio\ AM\ to\ control = \frac{Average\ \Delta W/A_o\ AM}{Average\ \Delta W/A_o\ control} = \frac{3.16277}{0.673437} = 4.69646$$

4.2 Topographical Analysis

The initial and final topography of the samples were compared to detect changes produced by effect of the corrosion. Figures 14 to 16 show the level maps of representative samples. Some changes in the morphology can be observed on the surface and the edges of the samples. The dispersed darker color areas on the surface (circled on Figs. 14 and 15) potentially indicate sites of accumulation of oxide, and the changes in tonalities suggest the formation of a passive oxide layer. Also, an increase in the size of pits was identified, as it can be seen on Figure 15 (small oval on the right). These characteristics are observed particularly on the additively manufactured samples. The control samples present smoother surfaces, which is expected since they were originally smoother due to their manufacturing process.

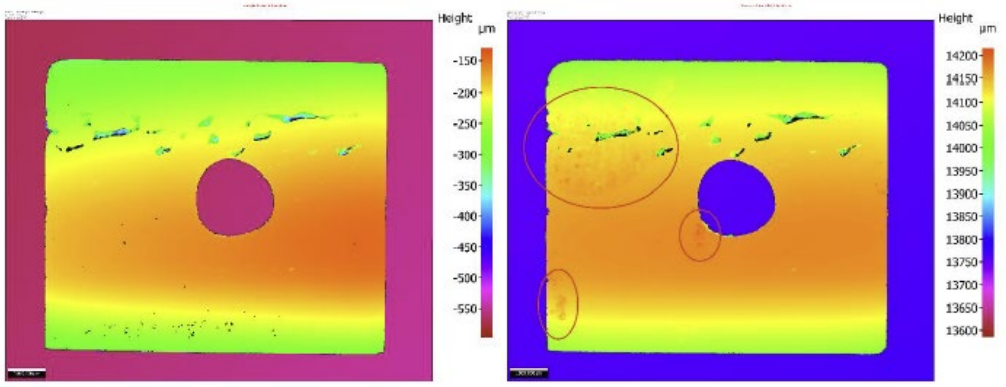

Figure 14: AM sample 3 initial (left) and final (right) surface map.

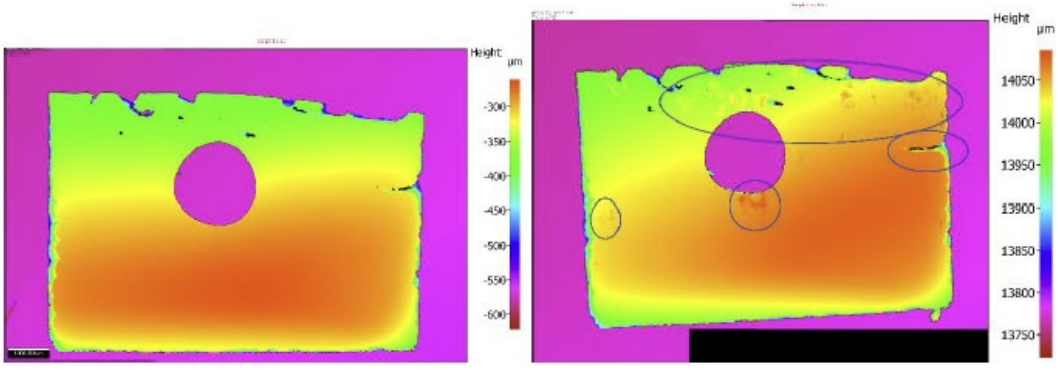

Figure 15: AM sample 1 initial (left) and final (right) surface map.

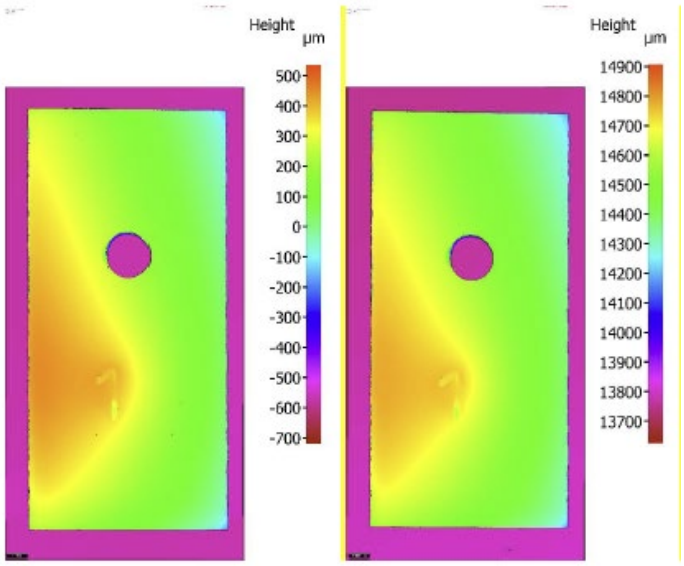

Figure 16: Control sample 1 initial (left) and final (right) surface map.

4.3 Visual Evaluation: Macroscopic Inspection, Optical Microscopy, and Scanning Electron Microscopy

4.3.1 After 12 Hours of Exposure

Some oxide coloration was observed at different grades on the additively manufactured samples (Fig. 17). No loose oxide particles were detected, but a thin not uniform layer of oxide well attached to the surface. It was noticed that one face of each sample presented more corrosion than the other face. This could be related to the orientation of the samples, which were hanging at an angle. To avoid this variation, the wire used for hanging the samples was replaced for a thinner one which extended straight downward, allowing the samples to hang vertically.

Control samples presented less visible corrosion macroscopically (Fig. 17). Observed both under the optical microscope and the scanning electron microscope, these samples showed circular formations of oxide. At higher magnification on the SEM, cubic formations could be observed in some dispersed areas (Fig. 18). Dendrites were observed on both the control samples and the additively manufactured (Fig. 19).

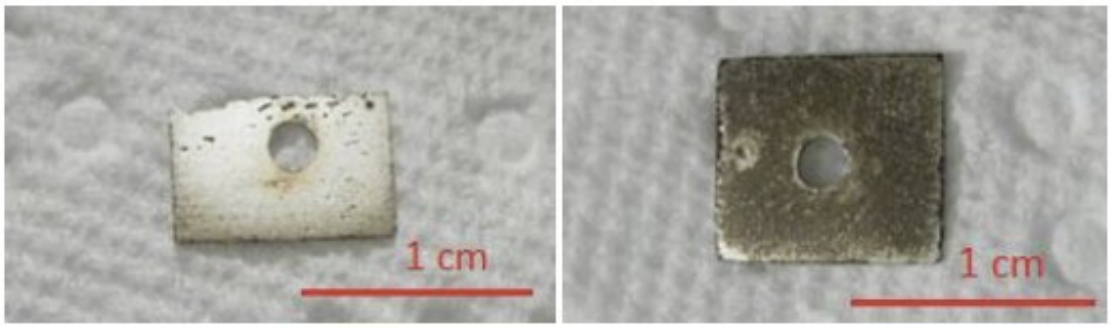

Figure 17: AM samples presenting different grades of oxide formation after 12 hours of exposure to the corrosive atmosphere.

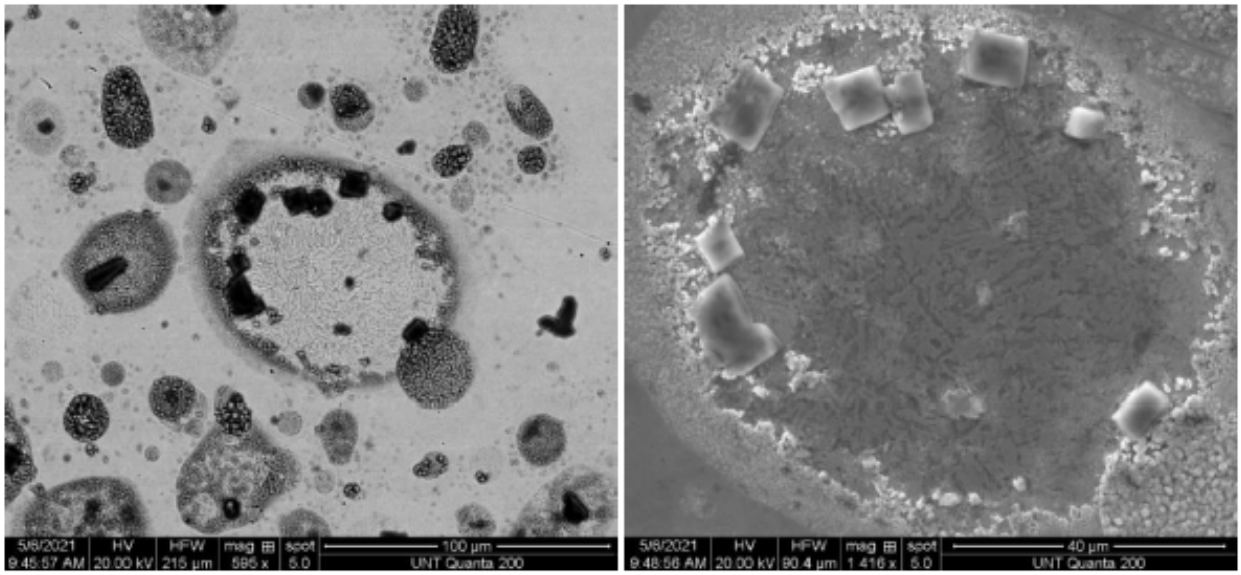

Figure 18: : Circular patterns observed on control sample in the scanning electron microscope. Some cubic formations (black on left picture, light gray on right) can be observed.

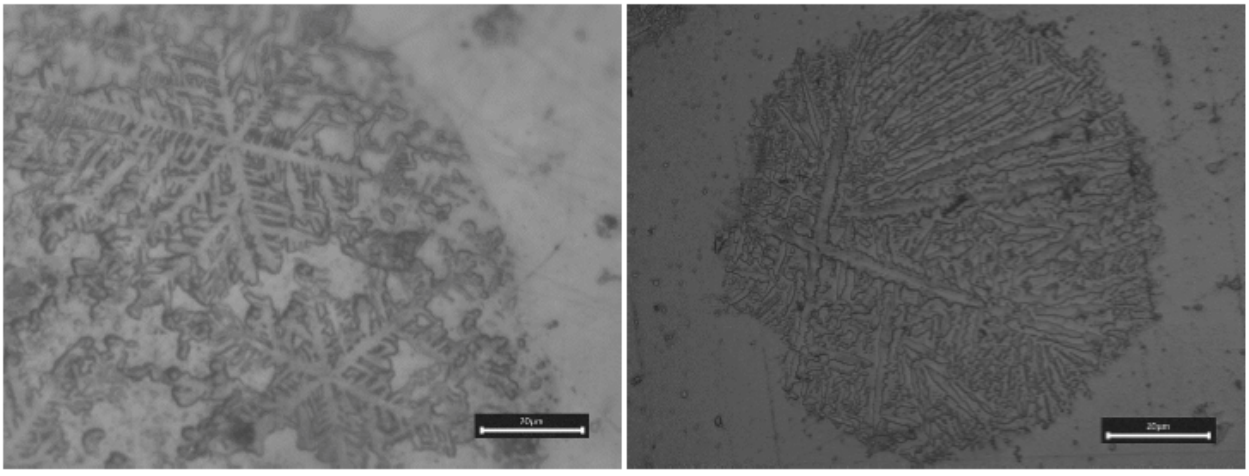

Figure 19: Dendrites observed on AM sample (left) and control sample (right).

4.3.2 After 310 Hours of Exposure

Observed under the optical microscope, the additively manufactured samples showed a greater amount of corrosion than the control samples (Fig. 20). At this stage of the corrosion test, the circular formations of oxide started to appear more densely clustered in big patches (Fig. 21) on several of the additively manufactured samples. The control samples showed oxide formations and apparent material dissolution near dendrites (Fig. 21).

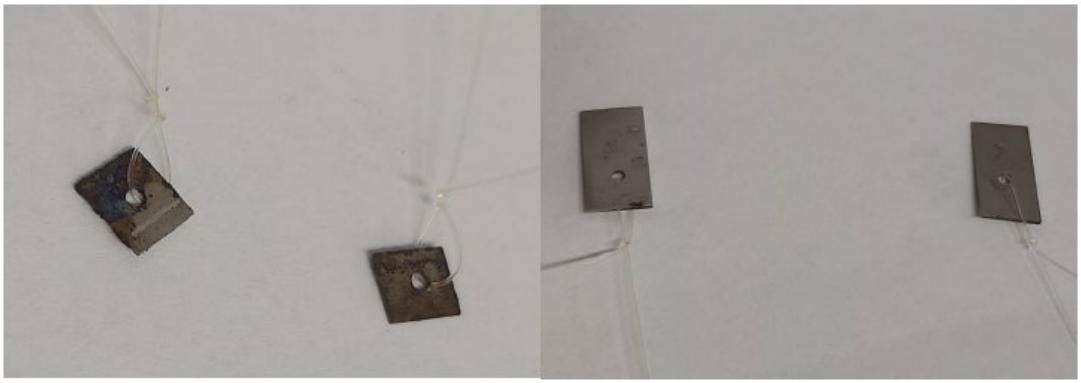

Figure 20: Test samples AM (left) and control (right) after 310 hours of exposure to corrosive atmosphere.

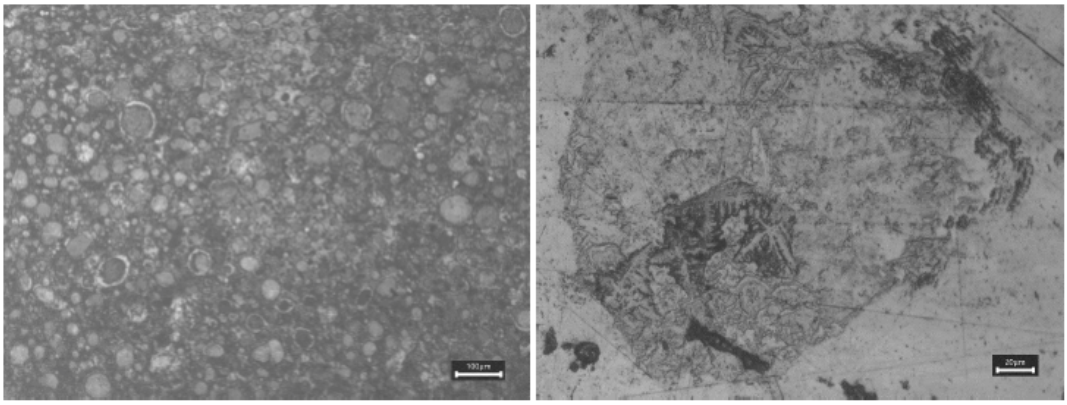

Figure 21: Patches of circular oxide formations on AM samples (left). Oxide surrounding a zone of dendrites and apparent material dissolution (pit) on control sample (right).

On the scanning electron microscope, a more severe material loss was observed on the additively manufactured samples; this damage was more evident in areas close to edges

(perimeter of the samples or around the hole) and the damaged areas presented spherical shapes (Fig. 22). On the control samples, deposits of cubic particles of oxide were observed in several areas (Fig. 23).

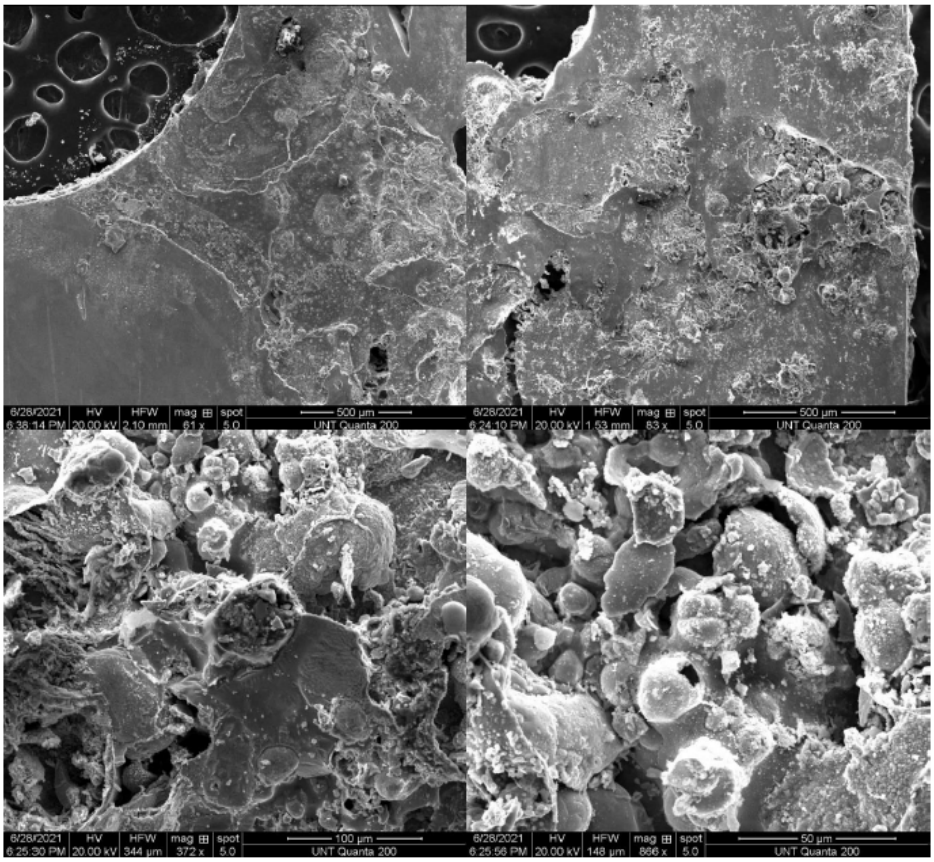

Figure 22: Material loss observed on AM samples, mostly on areas close to edges, after 310 hours of exposure to corrosive atmosphere.

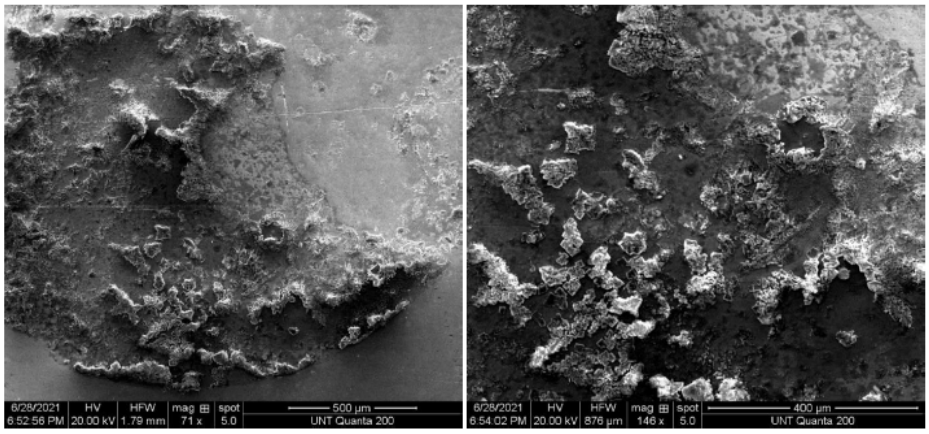

Figure 23: Clusters of cubical shaped oxide deposits on control samples.

4.3.3 After 635 Hours of Exposure

After the final stage of the corrosion test, it was observed in the macroscopic inspection that the additively manufactured samples had a much higher level of corrosion than the control samples. The additively manufactured samples presented a darkened shiny surface with varying coloration (Fig. 24) and a small amount of loose oxide particles. The control samples presented an incipient reddish and grayish tone with dark stains in some areas, with no loose oxide particles (Fig. 24).

Figure 24: AM and control samples after 635 hours under corrosive atmosphere. AM presented different colorations with a shiny finish (left). Control presented a reddish and grayish finish (right).

Observed under the optical microscope, it could be seen that the additively manufactured samples presented increased zones with material loss and high accumulation of patchy black oxide, particularly at their corners (Fig. 25). The size and quantity of pits and crevices was bigger than during the previous stages of the test, as it can be seen on Figure 26. These damages were observed too with the scanning electron microscope spotting zones with cracked material and many pits (Fig. 27). Another interesting finding on these same samples was complex clusters of acicular fiber shaped material on areas with high damage (Fig. 28). It were also observed areas of dissolved material (voids) surrounding dendrites and pits initiating in the vicinity of dendrites (Figs. 29 and 30).

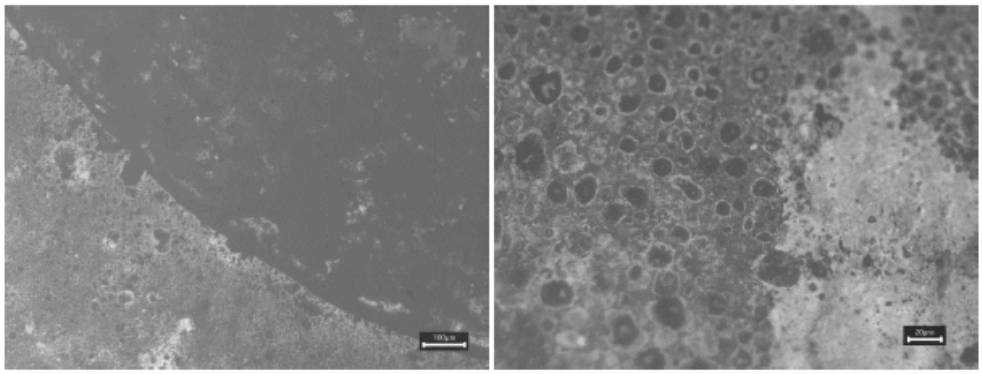

Figure 25: Corner of AM sample 3 showing a big dark corroded area (left). Patchy oxide formation with circular shapes on the corroded area (right).

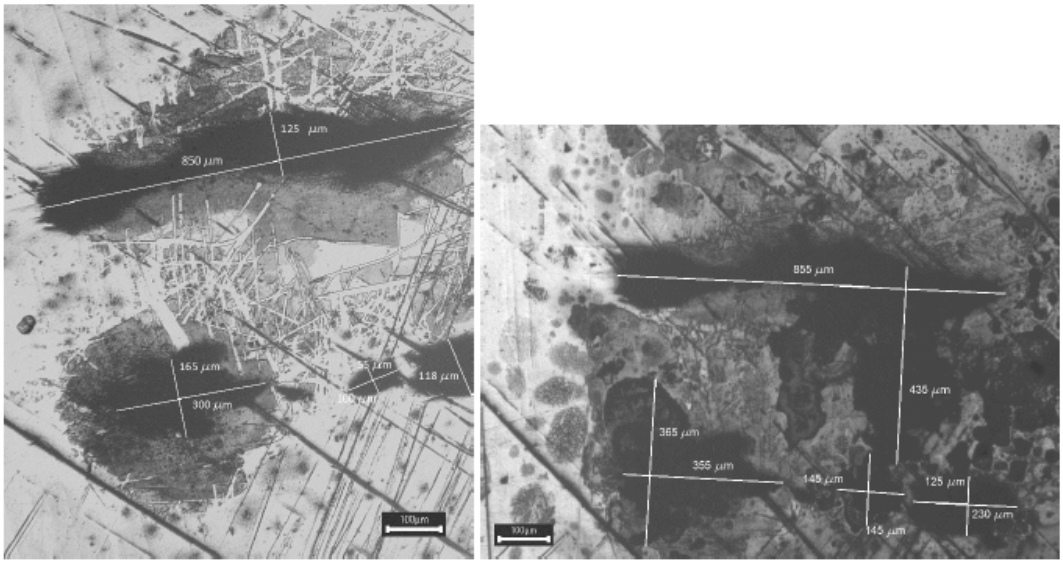

Figure 26: Pits on AM sample 4 after 12 hours (left) and 635 hours (right) of exposure to the corrosive atmosphere. A great increase in the size of pits is observed.

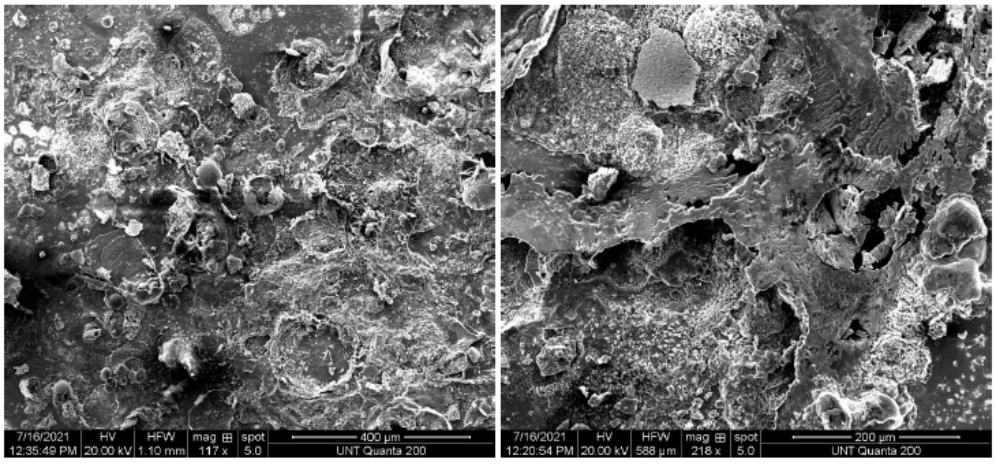

Figure 27: Cracked layer of material and pits on AM sample.

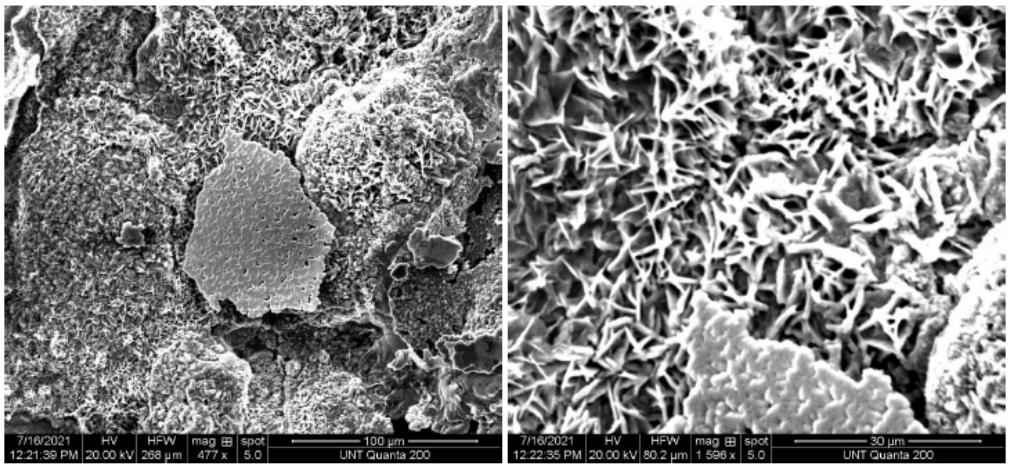

Figure 28: Cluster of acicular branched formations of oxide, potentially whiskers of oxyhydroxide, on AM sample.

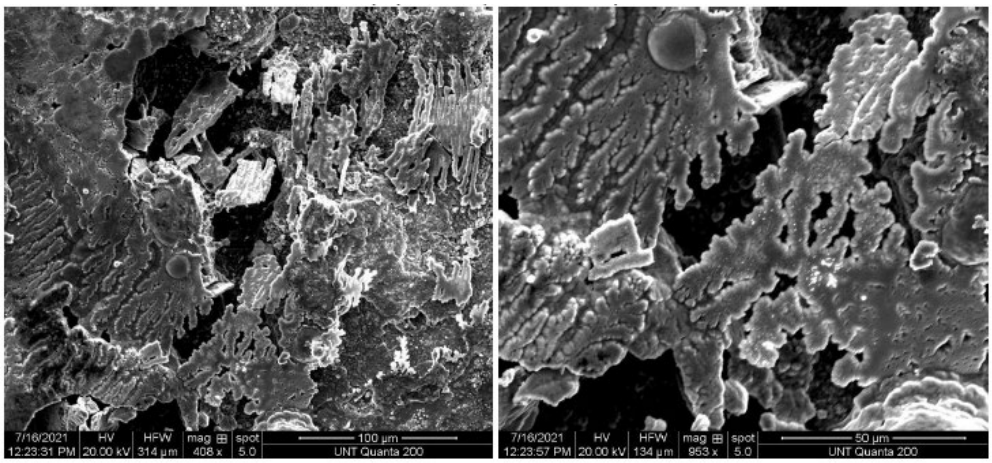

Figure 29: Dendrites presenting material loss around them on AM samples.

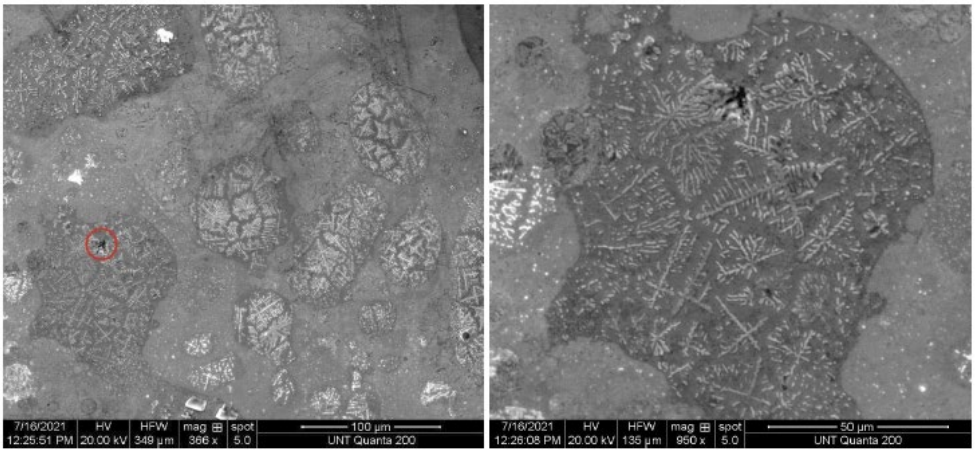

Figure 30: Some pits within areas of dendrites were observed with the SEM on the AM samples, potentially indicating zones more prone to damage by corrosion.

On the control samples no zones of great damage were identified, but some whitish circular areas with cubic structures within them were observed, potentially oxides (Fig. 31). Also, some dendrites protruding from the surface were seen.

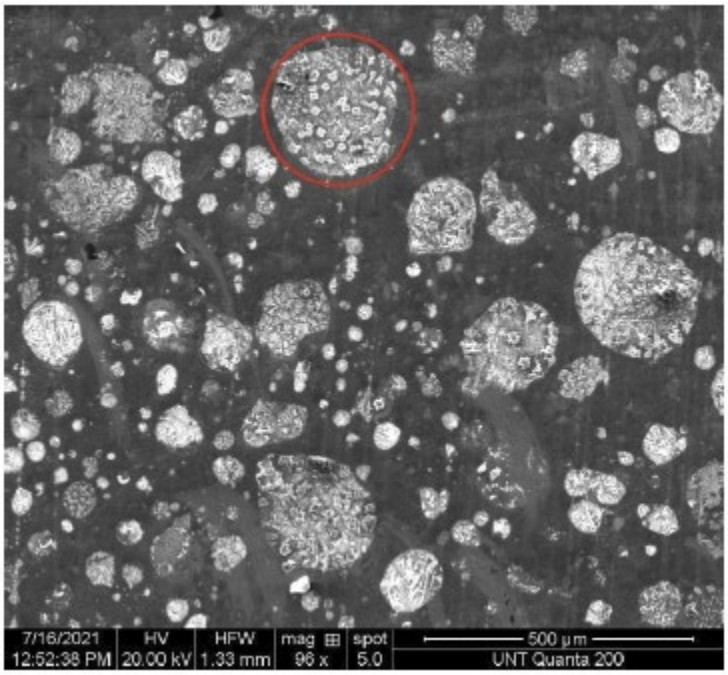

Figure 31: Cubic structures spotted on control samples, potentially oxides.

CHAPTER 5

DISCUSSION

5.1 Weight Loss Analysis

From the estimated ratio of weight loss per surface area between the AM samples and the control, it is evident that the AM were more severely affected by corrosion since their rate was 4.7 times bigger than the corresponding for control. From an engineering practical standpoint, corrosion is evaluated in terms of mils penetration per year (thousands of an inch per year), or the corresponding using SI units (µm/year, mm/year, etc.). Using the formulas of Equation 2 and Equation 3 presented by D. A. Jones [26], the corrosion rate for the additively manufactured samples and the control samples was calculated in terms of MPY (mils per year) and µm/year; this allows to have a clearer idea of the impact of the corrosion on a material in use.

$$MPY = \frac{534\,W}{\rho AT} \qquad \text{Eq. 2 [26]}$$

$$\frac{\mu m}{year} = \frac{87600\,W}{\rho AT} \qquad \text{Eq. 3 [26]}$$

In both formulas, W represents the weight loss in milligrams (mg), ρ represents the density of the metal in grams per cubic centimeter (g/cm^3), and T represents the time in hours. A represents the area, in square inches (in^2) for the MPY case and in square centimeters (cm^2) for the µm/year formula.

The rates of corrosion penetration calculated and their averages for the additively manufactured and control samples are shown on Table 12 and Table 13. If we calculate the AM to control ratio for the corrosion penetration we get:

$$Corr.penetration\ ratio\ AM\ to\ control = \frac{Avg\ MPY\ AM}{Avg\ MPY\ control} = \frac{0.215247}{0.045841} = 4.69551$$

$$Corr.penetration\ ratio\ AM\ to\ control = \frac{Avg\ \mu m/year\ AM}{Avg\ \mu m/year\ control} = \frac{5.47308}{1.16559} = 4.69554$$

As it can be seen, the results in both units are consistent, and they are also consistent to the ratio of weight loss per surface area which yielded a value of 4.69646.

Table 12: Rates of corrosion penetration estimated for AM samples.

Sample	MPY	µm/year
AM2	0.224184	5.70032
AM3	0.149386	3.79844
AM4	0.272171	6.92049
Average	0.215247	5.47308

Table 13: Rates of corrosion penetration estimated for control samples.

Sample	MPY	µm/year
Control 1	0.047187	1.19981
Control 2	0.047143	1.1987
Control 3	0.031795	0.808442
Control 4	0.057239	1.45541
Average	0.045841	1.16559

It is relevant to remark that both kind of samples performed outstandingly according to the reference for evaluation of corrosion rates presented by D. A. Jones [26]. According to the mentioned source, rates of corrosion smaller than 1 MPY or smaller than 25 µm/year represent an outstanding performance of the material, in a scale of: unacceptable, poor, fair, good, excellent, and outstanding. These results mean that the additively manufactured samples will be losing 0.0002 inches of thickness per year or 0.0055 mm of thickness per year, while the control samples will be losing 0.00005 inches of thickness per year or 0.0012 mm of thickness per year.

A schematic showing the practical explanation of this corrosion quantification method is shown on Figure 32. Nevertheless, it is important to consider that these estimations are for uniform corrosion of a surface without defects. In a real situation, the defects initially present on a sample, promote more aggressive mechanisms of corrosion, like pitting, that can make a material fail at a specific point. For these calculations the density of 316L stainless steel from the manufacturer EOS was used as reference because this property is not reported in the specifications sheet from the manufacturer of the powder used (LPW) and the material from EOS is cited as similar in the same specifications sheet. The properties of 316L from EOS were obtained from the material property database Matweb [27].

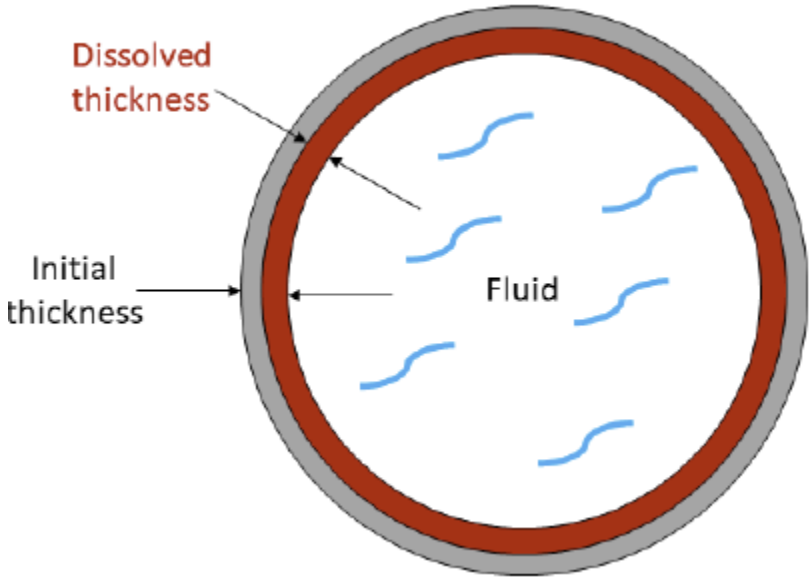

Figure 32: Schematic showing the application of the corrosion quantification method presented in source [26]. It must be noted that it considers only the effect of uniform corrosion.

5.2 Topographical Analysis

The results from the topographical analysis show the presence of some apparent oxide clusters on the long surfaces of the samples after the corrosion test, as it is noted on the surface

maps. These maps also show that a slight increase in the thickness of the samples occurred, which is not surprising since it matches the hypothesis of the protective oxide layer formation; the increase in the thickness can be attributed to the formation of this oxide on the surface. Some changes could be identified on the edges of the samples, which are more prone to suffer corrosion because of their rougher surface finish and their shape (edges are points of stress concentration).

Another important point to note about the topographical analysis results is the smoother surface finish of the control samples, which is due to their manufacturing process. Parts made through directed energy deposition naturally present rough surfaces and small gaps can be present in the material between the deposited tracks. If the first did not play a role in this case since all the samples were sanded and polished, the second was observed in the form of cracks and pits on the surface. These defects act as points of accelerated corrosion through anodic dissolution and potentially contributed to the weight loss. This could have been detected on the surface analysis by measuring the depth of pits and cracks before and after the corrosion test, but the scans did not have the enough depth of field to capture the surface inside these defects, a possible limitation of the technology which has been previously reported [4].

5.3 Visual Evaluation

The outcomes of the visual evaluation of the samples with the three techniques that were implemented (macroscopical inspection, optical microscopy, and scanning electron microscopy) show that the additively manufactured (AM) samples suffered more corrosion than the control samples; these results are aligned with the results of weight loss and topographical evaluation. However, there are some relevant remarks and findings from this visual inspection. The

additively manufactured samples presented mainly acicular oxide structures, which correspond to oxyhydroxides. Control samples, besides acicular structures, presented cubic structures which correspond to oxides. In both cases, the oxide layer presented good adherence to the metal, with minimal loose particles after the first three stages of the corrosion test. During the fourth and fifth stages, although a minimal quantity of corrosion material could be collected from the surface of the samples, cracked material could be observed with scanning electron microscopy on the additively manufactured, indicating the presence of loose oxide (Fig. 27). Control samples remained without loose oxide along the entirety of the test.

The greater amount of corrosion of the additively manufactured samples can be related to several factors. One possible factor is the presence of cracks and pits on the initial state (as manufactured) of the test samples compared to the smooth flat surface of the control samples. As it was previously mentioned, these defects provide sites for a more aggressive corrosion attack. Besides the macroscopically visible pits and cracks, due to the deposition process mechanism, additional microscopic pits that were observed during the visual inspection (Figs. 26, 27, and 30) decrease the corrosion resistance of the material. These microscopic pits are product of the inclusion of oxides in the matrix of the material which have been reported as a common characteristic in 316L stainless steel produced through both conventional and additive manufacturing methods [9]. These oxides, which have been identified by several researches reported by Saboori [9], are known to promote intergranular corrosion when their constituting atoms migrate to grain boundaries to form chromium carbide by the effect of sensitization of the material, and consequently forming zones of chromium depletion. When the corrosive agent attacks those unprotected zones it initiates pits, as it had been reported by Ganesh et al. [18].

Another possible factor is the higher energy stored in the AM material due to its faster cooling rate during deposition compared to the casting and rolling process of the control samples. That stored energy promotes faster reactions in the material to reach a more stable state, thus oxidizing it. This faster cooling rate also produces finer microstructures with dendrites; in the observations with the scanning electron microscope (SEM) some areas of dendrites were found to be suffering a severe material loss and formation of pits (Figs. 29 and 30). In the previously mentioned research conducted by Ganesh [18], the dendrites were identified as preferential sites for initiation of pitting corrosion, along with grain boundaries. More and bigger dendrites were observed on the AM samples than on the control samples and this is expected due to their manufacturing process, as previously mentioned. Based on the observations and the previous works cited [18], it is inferred that the dendritic microstructure is another factor that affected the performance of the AM samples in the corrosion test.

It is important to mention that the microstructure of parts produced by directed energy deposition (DED) can be controlled to some point by adjusting the process parameters of the deposition to control the cooling rate of the molten metal, and by using different metal powder particle sizes which have been identified to have an impact in the microstructure obtained [24].

CHAPTER 6

CONCLUSIONS

The additively manufactured 316L stainless steel proved good resistance against corrosion in an environment of elevated temperature and humidity, judging from the results obtained for the rate of corrosion penetration. Nevertheless, it did not perform better than the material produced by conventional method (casting and rolling), since the corrosion rate of the control samples was around 4.7 times smaller both in terms of weight loss per surface area and in corrosion penetration.

Although the additively manufactured samples showed more damage due to corrosion than the control samples (manufactured by conventional method), they still presented a shiny surface finish, indicating the formation of a passive oxide layer. The microscopic analysis allowed to identify the increase in size and number of pits and crevices; these two findings together allow to conclude that the material dissolution was focalized on the defects, many of them initially present in the AM samples due to a not optimal deposition process.

An optimization of parameters of the directed energy deposition process of 316L stainless steel (process used for the production of the additively manufactured samples for this test) is necessary to get a material with a higher resistance to corrosion, competitive to the material produced through conventional method. Besides the parameters controlled for the present research, the use of a metal powder with a different particle size would be recommended. Altogether, these parameters have an impact macroscopically in the production of a denser material with consistent tracks with low porosity and without gaps, and good track overlap; and

microscopically in the microstructure produced, which affects the mechanical properties and corrosion resistance.

The main contributions of this research are:

- It establishes a reference for other investigations on the corrosion resistance of additively manufactured 316L stainless steel made by directed energy deposition.
- It provides a reference for assessing the capabilities of directed energy deposition of 316L stainless steel.
- It provides a reference for evaluating the technical feasibility of implementing directed energy deposition as a technology for the manufacture of components of industrial flow systems. It serves as a reference for valves and piping manufacturers, who are considering additive manufacturing for the production of their parts.
- It serves as a reference for the industry in efforts of implementing more efficient methods for the repair of components.

CHAPTER 7

FUTURE WORK

The following activities are recommended to expand the scope of the research presented in this publication:

- Characterization of the oxide products by energy dispersive X-ray spectroscopy and Fourier transform infrared spectroscopy, to better understand the differences in the behavior between the AM and control samples.
- Optimization of directed energy deposition parameters to obtain parts with a morphology and microstructure more resistant to corrosion, including the use of metal powder with different particle size.
- Performance a of more extensive corrosion test to obtain more oxide deposits and collect the material for chemical composition analysis to identify the oxide products.
- Performance of a more intensive surface morphology characterization of the samples, to evaluate the progression of growth of pits in size and depth.
- Study on the formation of the passive oxide layer in materials made by directed energy deposition and its impact on the rate of weight loss along the exposure time.
- Optimization of directed energy deposition parameters to achieve the production of overhang shapes (without supporting material) that allow the manufacture of components of flow systems.
- Optimization of directed energy deposition parameters to obtain a successful deposition over grooves (no supporting material) to extend the research to the development of a method for repair of valves and piping elements.

- Testing of parts manufactured or repaired with directed energy deposition technology, under severely corrosive conditions like rapid flow, high temperature steam, or under presence of highly corrosive agents, to assess the feasibility of application of this technology for the production and repair of industrial parts.

APPENDIX

COMPLETE DATA FROM SAMPLE WEIGHT MEASUREMENT

Table A.1: Initial weights of additively manufactured (AM) samples.

Stage	Initial			
Sample	~~1~~	2	3	4
Weight (g)	~~0.0882~~	0.1804	0.1586	0.1667
	~~0.0878~~	0.1808	0.1586	0.1664
	~~0.0881~~	0.1806	0.1588	0.1669
	~~0.0884~~	0.1805	0.1582	0.1667
	~~0.0880~~	0.1807	0.1587	0.1665
Average	~~0.0881~~	0.1806	0.1586	0.1666

Table A.2: Weights of AM samples after 12 hours under corrosive atmosphere.

Stage	After 12 hours			
Sample	~~1~~	2	3	4
Weight (g)	~~0.0879~~	0.1797	0.1578	0.1653
	~~0.0883~~	0.1807	0.1587	0.1663
	~~0.0880~~	0.1803	0.1582	0.1666
	~~0.0880~~	0.1806	0.1585	0.1662
	~~0.0879~~	0.1801	0.1584	0.1664
Average	~~0.0880~~	0.1803	0.1583	0.1662

Table A.3: Weights of AM samples after 36 hours under corrosive atmosphere.

Stage	After 36 hours			
Sample	~~1~~	2	3	4
Weight (g)	~~0.0882~~	0.1803	0.1585	0.1663
	~~0.0880~~	0.1804	0.1585	0.1665
	~~0.0882~~	0.1804	0.1581	0.1664
	~~0.0883~~	0.1801	0.1587	0.1664
	~~0.0877~~	0.1801	0.1583	0.1664
Average	~~0.0881~~	0.1803	0.1584	0.1664

Table A.4: Weights of AM samples after 84 hours under corrosive atmosphere.

Stage	After 84 hours			
Sample	~~1~~	2	3	4
Weight (g)	~~0.0881~~	0.1803	0.1582	0.1666
	~~0.0880~~	0.1802	0.1585	0.1665
	~~0.0881~~	0.1803	0.1584	0.1666
	~~0.0883~~	0.1803	0.1585	0.1666
	~~0.0882~~	0.1801	0.1586	0.1666
Average	~~0.0881~~	0.1802	0.1584	0.1666

Table A.5: Weights of AM samples after 310 hours under corrosive atmosphere.

Stage	After 310 hours			
Sample	~~1~~	2	3	4
Weight (g)	~~0.0878~~	0.1805	0.1583	0.1664
	~~0.0880~~	0.1800	0.1571	0.1660
	~~0.0874~~	0.1800	0.1582	0.1660
	~~0.0886~~	0.1797	0.1576	0.1655
	~~0.0884~~	0.1804	0.1582	0.1660
Average	~~0.0880~~	0.1801	0.1579	0.1660

Table A.6: Weights of AM samples after 635 hours under corrosive atmosphere.

Stage	After 635 hours			
Sample	~~1~~	2	3	4
Weight (g)	~~0.0874~~	0.1800	0.1583	0.1661
	~~0.0877~~	0.1802	0.1584	0.1656
	~~0.0878~~	0.1803	0.1582	0.1660
	~~0.0880~~	0.1800	0.1581	0.1662
	~~0.0877~~	0.1799	0.1583	0.1662
Average	~~0.0877~~	0.1801	0.1583	0.1660

Table A.7: Initial weights of control samples.

Stage	Initial			
Sample	1	2	3	4
Weight (g)	1.0527	1.1375	0.9345	1.0176
	1.0525	1.1381	0.9341	1.0176
	1.0530	1.1378	0.9345	1.0172
	1.0528	1.1378	0.9345	1.0168
	1.0532	1.1380	0.9345	1.0172
Average	1.0528	1.1378	0.9344	1.0173

Table A.8: Weights of control samples after 12 hours under corrosive atmosphere.

Stage	After 12 hours			
Sample	1	2	3	4
Weight (g)	1.0529	1.1373	0.9343	1.0172
	1.0528	1.1375	0.9341	1.0171
	1.0527	1.1374	0.9345	1.0172
	1.0529	1.1377	0.9340	1.0172
	1.0525	1.1376	0.9343	1.0170
Average	1.0528	1.1375	0.9342	1.0171

Table A.9: Weights of control samples after 36 hours under corrosive atmosphere.

Stage	After 36 hours			
Sample	1	2	3	4
Weight (g)	1.0532	1.1377	0.9343	1.0171
	1.0526	1.1376	0.9346	1.0172
	1.0531	1.1377	0.9344	1.0170
	1.0529	1.1376	0.9347	1.0169
	1.0528	1.1377	0.9342	1.0173
Average	1.0529	1.1377	0.9344	1.0171

Table A.10: Weights of control samples after 84 hours under corrosive atmosphere.

Stage	After 84 hours			
Sample	1	2	3	4
Weight (g)	1.0530	1.1377	0.9343	1.0171
	1.0529	1.1376	0.9342	1.0175
	1.0531	1.1378	0.9345	1.0176
	1.0529	1.1379	0.9345	1.0175
	1.0529	1.1380	0.9344	1.0172
Average	1.0530	1.1378	0.9344	1.0174

Table A.11: Weights of control samples after 310 hours under corrosive atmosphere.

Stage	After 310 hours			
Sample	1	2	3	4
Weight (g)	1.0526	1.1376	0.9340	1.0166
	1.0525	1.1377	0.9337	1.0165
	1.0527	1.1375	0.9335	1.0167
	1.0526	1.1375	0.9338	1.0165
	1.0526	1.1378	0.9338	1.0165
Average	1.0526	1.1376	0.9338	1.0166

Table A.12: Weights of control samples after 635 hours under corrosive atmosphere.

Stage	After 635 hours			
Sample	1	2	3	4
Weight (g)	1.0524	1.1376	0.9342	1.0168
	1.0526	1.1376	0.9341	1.0167
	1.0525	1.1375	0.9343	1.0171
	1.0525	1.1376	0.9342	1.0170
	1.0527	1.1374	0.9343	1.0170
Average	1.0525	1.1375	0.9342	1.0169

REFERENCES

[1] ISO/ASTM International, “ISO/ASTM 52900: Additive manufacturing - General principles and Terminology,” *Int. Stand.*, vol. 5, no. 978-84-9042-335–6, pp. 1–26, 2015, [Online]. Available: https://www.iso.org/obp/ui/#iso:std:69669:en%0Ahttps://www.iso.org/standard/69669.html%0Ahttps://www.astm.org/Standards/ISOASTM52900.htm.

[2] M. P. Sealy, G. Madireddy, R. E. Williams, P. Rao, and M. Toursangsaraki, “Hybrid processes in additive manufacturing,” *J. Manuf. Sci. Eng. Trans. ASME*, vol. 140, no. 6, 2018, doi: 10.1115/1.4038644.

[3] A. Manufacturing and A. T. A. Sy, “Advancing Thermal Management Advancing Thermal Management.”

[4] A. Townsend, N. Senin, L. Blunt, R. K. Leach, and J. S. Taylor, “Surface texture metrology for metal additive manufacturing: a review,” *Precis. Eng.*, vol. 46, pp. 34–47, 2016, doi: 10.1016/j.precisioneng.2016.06.001.

[5] A. Thompson, N. Senin, C. Giusca, and R. Leach, “Topography of selectively laser melted surfaces: A comparison of different measurement methods,” *CIRP Ann. - Manuf. Technol.*, vol. 66, no. 1, pp. 543–546, 2017, doi: 10.1016/j.cirp.2017.04.075.

[6] F. Cabanettes *et al.*, “Topography of as built surfaces generated in metal additive manufacturing: A multi scale analysis from form to roughness,” *Precis. Eng.*, vol. 52, no. October 2017, pp. 249–265, 2018, doi: 10.1016/j.precisioneng.2018.01.002.

[7] A. Keshavarzkermani *et al.*, “An investigation into the effect of process parameters on melt pool geometry, cell spacing, and grain refinement during laser powder bed fusion,” *Opt. Laser Technol.*, vol. 116, pp. 83–91, Aug. 2019, doi: 10.1016/j.optlastec.2019.03.012.

[8] A. Saboori *et al.*, “An investigation on the effect of powder recycling on the microstructure and mechanical properties of AISI 316L produced by Directed Energy Deposition,” *Mater. Sci. Eng. A*, vol. 766, no. August, p. 138360, 2019, doi: 10.1016/j.msea.2019.138360.

[9] A. Saboori, A. Aversa, G. Marchese, S. Biamino, M. Lombardi, and P. Fino, “Microstructure and Mechanical Properties of AISI 316L Produced by Directed Energy Deposition-Based Additive Manufacturing: A Review,” *Appl. Sci.*, vol. 10, no. 9, p. 3310, May 2020, doi: 10.3390/app10093310.

[10] AMFG, “An Introduction to Wire Arc Additive Manufacturing [2020 Update] - AMFG,” 2020. https://amfg.ai/2018/05/17/an-introduction-to-wire-arc-additive-manufacturing/ (accessed Aug. 01, 2021).

[11] L. Wang, J. Xue, and Q. Wang, “Correlation between arc mode, microstructure, and mechanical properties during wire arc additive manufacturing of 316L stainless steel,” *Mater. Sci. Eng. A*, vol. 751, pp. 183–190, Mar. 2019, doi: 10.1016/j.msea.2019.02.078.

[12] B. Wu *et al.*, “A review of the wire arc additive manufacturing of metals: properties, defects and quality improvement,” *J. Manuf. Process.*, vol. 35, pp. 127–139, 2018, doi: 10.1016/j.jmapro.2018.08.001.

[13] X. Lou, M. A. Othon, and R. B. Rebak, “Corrosion fatigue crack growth of laser additively-manufactured 316L stainless steel in high temperature water,” *Corros. Sci.*, vol. 127, no. June, pp. 120–130, 2017, doi: 10.1016/j.corsci.2017.08.023.

[14] X. Lou, M. Song, P. W. Emigh, M. A. Othon, and P. L. Andresen, “On the stress corrosion crack growth behaviour in high temperature water of 316L stainless steel made by laser powder bed fusion additive manufacturing,” *Corros. Sci.*, vol. 128, no. September, pp. 140–153, 2017, doi: 10.1016/j.corsci.2017.09.017.

[15] A. H. Bagheri, S. Nasrazadani, and H. Bostanci, “Impact of Internal Pipe Grooves on Flow-Accelerated Corrosion of Small-Bore A-106 Carbon Steel Pipes,” *J. Fail. Anal. Prev.*, vol. 17, no. 3, pp. 417–425, 2017, doi: 10.1007/s11668-017-0237-z.

[16] V. Kain, “Flow accelerated corrosion: Forms, mechanisms and case studies,” in *Procedia Engineering*, Jan. 2014, vol. 86, pp. 576–588, doi: 10.1016/j.proeng.2014.11.083.

[17] P. Dhaiveegan, N. Elangovan, T. Nishimura, and N. Rajendran, “Corrosion behavior of 316L and 304 stainless steels exposed to industrial-marine-urban environment: Field study,” *RSC Adv.*, vol. 6, no. 53, pp. 47314–47324, 2016, doi: 10.1039/c6ra04015b.

[18] P. Ganesh *et al.*, “Studies on pitting corrosion and sensitization in laser rapid manufactured specimens of type 316L stainless steel,” *Mater. Des.*, vol. 39, pp. 509–521, Aug. 2012, doi: 10.1016/J.MATDES.2012.03.011.

[19] G. Ko, W. Kim, K. Kwon, and T. K. Lee, “The corrosion of stainless steel made by additive manufacturing: A review,” *Metals (Basel).*, vol. 11, no. 3, pp. 1–21, 2021, doi: 10.3390/met11030516.

[20] M. Wang, S. Zeng, H. Zhang, M. Zhu, C. Lei, and B. Li, “Corrosion behaviors of 316 stainless steel and Inconel 625 alloy in chloride molten salts for solar energy storage,” *High Temp. Mater. Process.*, vol. 39, no. 1, pp. 340–350, 2020, doi: 10.1515/htmp-2020-0077.

[21] M. J. K. Lodhi, K. M. Deen, and W. Haider, “Corrosion behavior of additively manufactured 316L stainless steel in acidic media,” *Materialia*, vol. 2, no. May, pp. 111–121, 2018, doi: 10.1016/j.mtla.2018.06.015.

[22] N. S. Al-Mamun, W. Haider, and I. Shabib, “Corrosion resistance of additively manufactured 316L stainless steel in chloride−thiosulfate environment,” *Electrochim. Acta*, vol. 362, 2020, doi: 10.1016/j.electacta.2020.137039.

[23] R. I. Revilla *et al.*, “Microstructure and corrosion behavior of 316L stainless steel prepared using different additive manufacturing methods: A comparative study bringing insights into the impact of microstructure on their passivity,” *Corros. Sci.*, vol. 176, no. May, p. 108914, 2020, doi: 10.1016/j.corsci.2020.108914.

[24] W. Chen, G. Yin, Z. Huang, and Z. Feng, “Effect of the particle size of 316L stainless steel on the corrosion characteristics of the steel fabricated by selective laser melting,” *Int. J. Electrochem. Sci.*, vol. 13, no. 11, pp. 10217–10232, 2018, doi: 10.20964/2018.11.11.

[25] J. Stašić and D. Božić, “Densification behavior of 316L-NiB stainless steel powder and surface morphology during selective laser melting process using pulsed Nd:YAG laser,” *Rapid Prototyp. J.*, vol. 25, no. 1, pp. 47–54, 2019, doi: 10.1108/RPJ-07-2017-0136.

[26] D. A. Jones, “Corrosion Rate Units and Calculations,” in *Principles and prevention of corrosion*, 2nd ed., Upper Saddle River, NJ: Prentice Hall, 1996, pp. 31–34.

[27] “EOS StainlessSteel 316L DMSL on EOS M 100.” http://matweb.com/search/DataSheet.aspx?MatGUID=5d6d18ea1a5648bdaaa442500dad52fa (accessed Aug. 09, 2021).